

# Hybrid vibration absorber with detached design for global vibration control

**M.H. TSO, J. YUAN, W.O. WONG**

*Department of Mechanical Engineering, The Hong Kong Polytechnic University,  
Hong Kong*

## **ABSTRACT**

A new hybrid vibration absorber (HVA), with detached passive and active parts, is designed, analyzed and tested. This is an alternative approach in case the traditional bundled HVA with collocated active and passive control elements cannot be applied. In fixed-free structures like buildings and towers, passive dynamic vibration absorber (DVA) is very popular for vibration control at or near the free-ends. Active control may be introduced to improve performance but spaces or weights may be limited in some applications. It may not be practical to attach an actuator near the passive part. The new approach provides more flexibility to retrofit a passive DVA into a high performance HVA by installing the actuator at a more suitable location than collocating with the passive part. The proposed HVA is based on the pole placement control strategy. Its controller is able to deal with a possible non-minimum phase secondary path caused by non-collocated actuator-sensors. This feature does not exist in a bundled HVA with collocated actuator-sensors. Performance of the new HVA is analyzed in this study. Experiment and simulation results are used to verify the theoretical results and demonstrate the excellent performance of the new HVA for vibration control at multiple points. A bundled HVA with collocated passive and active elements is compared with the proposed HVA with detached control elements using experimental and simulation results. It was found that the vibration attenuation performance of the proposed HVA can be better than the traditional bundled HVA. The optimal actuator location that is not necessarily the coupling point of the passive resonator can be selected numerically by a proposed procedure. One could miss a better solution for vibration control if he/she only uses the bundled HVA without considering the detached HVA as a possible alternative.

**Keywords:** System identification, Global vibration control, Vibration absorber, Hybrid control, Non-collocated, Detached absorber, Non-minimum phase

## 1. INTRODUCTION

Dynamic vibration absorber (DVA) is a well known device for vibration suppression (Hermann, 1909). It is very effective in suppressing narrowband vibration at the expense of an additional vibration peak in the closed-loop vibration power spectrum. Conventionally, a DVA is pre-tuned to a frequency for significant vibration suppression (Inman, 1994). Recently, there has been significant improvement in DVA design. It is theoretically possible to optimize one (Jacquot, 2003; Cheung and Wong, 2009) or multiple DVA's (Sun et al. 1995; Dayou and Brennan, 2002; Cha and Zhou, 2006; Cheung and Wong, 2008) to suppress multi-modal vibrations in flexible structures.

A possible way to improve the performance of DVA is to add an active element to form a hybrid vibration absorber (HVA) (Chang and Soong, 1980; Nishimura et al. 1989; Watanabe and Yoshida, 1994). Active control provides better capability on broadband vibration suppression. A HVA may be implemented as an inertial actuator when its passive part acts as a DVA, so that its active power consumption may be reduced (Watanabe and Yoshida, 1994; Lesieutre et al., 2003). An example of inertial actuator is a voice-coil. Inside the sealed case, the active element is mounted between the case and passive mass in parallel with the passive spring and damper (Chen et al., 2005). In practice, HVA and inertial actuators are popular for vibration control (Nonami et al., 1996). They are installed at those points without rigid supports within near ranges, such as tip or near tip positions of fixed-free structures. However, it is very important to reduce the mass ratio of DVA or HVA when one design these devices. If the suspended mass is reduced, actuation effects would also be reduced no matter how powerful an actuator is. A possible alternative may be to install the actuator at a point with rigid support nearby, so that it can exert maximum force/torque and achieve better control effects. There are other reasons, such as space or weight limits, for one to install the actuator at a better location than collocating with the suspended mass. It would be useful to engineers to have an alternative option to the traditional bundled HVA. The main contribution of this study is the exploration on how to design a detached HVA, how to select feedback sensor and actuator locations and how to design an active controller to deal with possible non-minimum-phase secondary path due to the un-collocated feedback sensor and actuator pair.

In the literature of HVA designs, most of them (Kosut, 1970; Nishimura et al., 1989) require accurate availability of eigen-functions and eigen-states of the primary structures. In reality, the eigen-functions may not be easily obtained with sufficient accuracy due to irregular shape and complicated boundary conditions of primary structures. Eigen-states with sufficient accuracy are also difficult to recover and require high cost as multi-channel signals are required (Balas, 1978). To avoid these practical problems, one may design an output feedback controller with collocated

sensor-actuators (Chang and Soong, 1980; Burdisso and Heilmann, 1998; Yuan, 2000). If collocated actuator-sensor is not permitted due to some unforeseeable problems or harsh environment (Daley and Wang, 2008) then the secondary control path may have a non-minimum phase problem. This problem can be solved with a pole placement controller. Its minimum requirement is a single actuator-sensor pair. This is a positive feature of the detached HVA. Many researchers apply a single HVA to attenuate vibration at a single point (Burdisso and Heilmann, 1998; Fujita et al., 1993; Olgac and Hansen, 1994; Kumagai et al. 1993), or multiple HVAs to attenuate vibration at multiple points (Yuan, 2001). It has been demonstrated recently the possibility of applying a single HVA with collocated passive and active elements for broadband and global structural vibration control (Tso et al., 2012 and 2013). To the best knowledge of the authors, this is the first report on HVA with detached active and passive parts for broadband and global vibration control of continuous structures. Both the detached HVA and its active control methodology are original results. A detached HVA may out-perform a bundled HVA, as demonstrated in our experimental and simulation verifications. A numerical procedure is proposed here to select the optimal actuator location that is not necessarily the coupling point of the passive resonator. One may miss a better solution for vibration control if he/she only uses the bundled HVA without considering the detached HVA as a possible alternative.

The organization of this paper is as follows. In Section 2, the governing equations of motion for the proposed HVA are derived. In Section 3, the design of the pole placement controller is addressed in detail. Experimental setup and results are presented in Sections 4 and 5 respectively, together with simulation results. Both experimental and simulation results verify the theoretical derivations and demonstrate good performance of the detached HVA for broadband and global structural vibration control. Finally, the conclusions are drawn in Section 7.

## 2. Configuration

The detached HVA consists of both active and passive elements. While the passive part may be a translational or rotational DVA, a rotational passive DVA is studied here. It is a pendulum-like device with a flexible beam as a rotational spring. A proper mechanism may be designed to adjust the distance between the suspended mass and the coupling point  $x=x_p$  on a primary structure as shown in Fig. 1a. Such a mechanism can be used to tune the DVA resonant frequency.

Similar to the typical installation of DVA in general fixed-free structures, the passive part of the detached HVA is coupled at the free end of a cantilever beam in the experimental study, i.e.  $x_p=L$ , where  $L$  is the length of the primary cantilever beam. The active element is a piezoelectric moment

bender which is detached from the passive element and may be installed on the beam at any suitable position  $x=x_a$ . The feedback sensor is a single axis translational accelerometer for measurement of transverse vibration. It is placed at  $x_p$ , the coupling point of the passive DVA, where vibration attenuation is most desired. Since amplitudes of all modes of the cantilever beam are in their maximum values at the structural tip position, the feedback signal measured at  $x_p=L$  is a reasonable choice in the experimental study.

For the system in Fig. 1a, transverse linear displacement of the primary structure is represented by  $w(x,t)$ . An equivalent disturbance  $r(t)\delta(x-x_d)$  exerts on the primary structure at position  $x=x_d$  where  $r(t)$  is a stationary random time function and  $\delta(x-x_d)$  is a Dirac delta function. Similarly,  $\tau_a(t)$  and  $\tau_p(t)$  describes the temporal effect of active and passive moments generated by the actuator and the DVA on the primary structure at  $x=x_a$  and  $x=x_p$  respectively. The primary structure is assumed to satisfy the Euler-Bernoulli hypothesis for displacement and Kelvin-Voigt damping hypothesis, with a dynamic equation

$$\rho\ddot{w}(x,t) + CI\dot{w}''''(x,t) + EIw''''(x,t) = \frac{\partial}{\partial x}[r(t)\delta(x-x_d)] + \frac{\partial}{\partial x}[\tau_p(t)\delta(x-x_p)] + \frac{\partial}{\partial x}[\tau_a(t)\delta(x-x_a)];$$

$$0 < x < L; \quad (1)$$

where  $\rho$ ,  $C$ ,  $I$  and  $E$  denote the mass per unit length, structural damping coefficient, second moment of cross sectional area of the primary structure and Young's modulus. Let  $\phi(t)$  and  $\theta(x,t)$  denote angular displacements of the DVA and the primary structure respectively. The coupling moment between the primary structure and the DVA is described by

$$\tau_p(t) = k[\phi(t) - \theta_p(t)] \quad (2)$$

where  $k$  is the spring stiffness and  $\theta_p(t) = \theta(x_p,t)$ . Coupling moment  $\tau_p(t)$  also drives the (rotational) motion of the pendulum such that

$$\tau_p(t) = -J\ddot{\phi}(t) \quad (3)$$

where  $J$  is the mass moment of inertia of the pendulum. One may express the linear displacement of the primary structure in modal space as

$$w(x,t) = \sum_{i=1}^{\infty} \varphi_i(x)\eta_i(t) \quad (4a)$$

where  $\varphi_i(x)$  is the  $i^{\text{th}}$  eigen-function of the primary structure. Angular displacement of the primary structure can be derived as

$$\theta(x,t) = -\frac{\partial w(x,t)}{\partial x} = -\sum_{i=1}^{\infty} \varphi_i'(x) \eta_i(t) \quad (4b)$$

where  $\varphi_i'(x) = \frac{d\varphi_i}{dx}$ . The translational velocity of the primary structure can be written as

$$v(x,t) = \dot{w}(x,t) = \sum_{i=1}^{\infty} \varphi_i(x) \dot{\eta}_i(t) \quad (4c)$$

The working principle of the new HVA can be explained with the help of Fig. 1 and Eqs. (1-4). For fixed-free structures like a cantilever beam, magnitude of vibration is maximum at the free-end, where vibration suppression is mostly desirable. Therefore the passive DVA is attached here. If an actuator is also mounted at the free-end, it is usually installed between the suspended mass and the primary structure. Typically, increasing the mass ratio will make the suspended mass approaching to a rigid support while reducing the mass ratio has an opposite effect. Therefore, the actuator may not be able to exert its maximum force/moment if reducing mass ratio is one of the design objectives. In the detached HVA, the actuator is allowed to be installed at another location. A possible choice of actuator location is as near any rigid support as possible, so that the actuator is able to exert stronger forces/moment for vibration suppression. For this reason, Eq. (1) contains two coupling moments, one passive and the other active, at separated locations. The passive coupling moment only applies to the suspended mass via Eqs. (2) and (3). The active coupling moment is explained in the next paragraph.

Besides location of the actuator, control algorithm is another issue. State feedback controllers are popular in active vibration control. It is not adopted here because state feedback  $\eta_i(t)$  requires multiple feedback sensors and accurate knowledge of eigen-functions  $\varphi_i(x)$ . In real applications, it is very difficult, if not impossible, to obtain accurate eigen-functions for the primary structures like buildings of towers with irregular shapes (cross-sections) or complicated boundary conditions. In this study, a translational velocity  $v_p(t) = \dot{w}(x_p, t)$  (measured at position  $x=x_p$  of the primary structure) is used as feedback to synthesize the active moment via an output feedback controller. In Laplace transform domain, the control law is

$$T_a(s) = G(s)V_p(s) \quad (5)$$

where  $T_d(s)$  and  $V_p(s)$  are the Laplace transform of  $\tau_a(t)$  and  $\dot{w}(x_p, t)$  respectively.  $G(s)$  is the controller transfer function to be discussed in later sections. For the closed-loop control system under active control, one may use  $\frac{V(x, s)}{R(s)}$  to represent the transfer function from the disturbance to any point  $x$  of the primary structure. In reality,  $R(s)$  can be either considered as an equivalent static wind load acting on a building or represented by a stationary random time function (Solari, 1988; Chen and Kareem, 2004). It is derived as Eq. (A14) in Appendix A and presented here in the following form:

$$\frac{V(x, s)}{R(s)} = \frac{-sK(s)B_{xd'}(s) + s^3\sqrt{kJ}\omega_a\Delta B_{xk}(s) + G(s)[s^2K(s)\Delta B_{xkG}(s) + s^4\sqrt{kJ}\omega_a\Delta B_{xkG}(s)]}{K(s)A(s) + s^2\sqrt{kJ}\omega_a B_{p'p'}(s) + G(s)[sK(s)B_{pa'}(s) + s^3\sqrt{kJ}\omega_a\Delta B_{kG}(s)]} \quad (6a)$$

Detailed definitions of  $K(s)$ ,  $A(s)$ ,  $B_{xd'}(s)$ ,  $\Delta B_{xk}(s)$ ,  $\Delta B_{xkG}(s)$ ,  $\Delta B_{xkG}(s)$ ,  $B_{p'p'}(s)$ ,  $B_{pa'}(s)$  and  $\Delta B_{kG}(s)$  are given as in Appendix A. One may focus on

$$D(s) = K(s)A(s) + s^2\sqrt{kJ}\omega_a B_{p'p'}(s) + G(s)[sK(s)B_{pa'}(s) + s^3\sqrt{kJ}\omega_a\Delta B_{kG}(s)] \quad (6b)$$

$$\text{and} \quad D(s) = Q(s) + G(s)M(s) \quad (6c)$$

where  $Q(s) = K(s)A(s) + s^2\sqrt{kJ}\omega_a B_{p'p'}(s)$ ,  $M(s) = [sK(s)B_{pa'}(s) + s^3\sqrt{kJ}\omega_a\Delta B_{kG}(s)]$ , and  $D(s)$  is the denominator polynomial of Eq. (6a) or the closed-loop characteristic equation. Its components,  $K(s)$ ,  $A(s)$ ,  $B_{p'p'}(s)$ ,  $B_{pa'}(s)$  and  $\Delta B_{kG}(s)$ , are all independent of spatial variable  $x$ . Dynamics of the primary structure, under active control, can have the same set of closed-loop poles (eigen-values), but different numerators with respect to different monitor positions  $x$ . This is seen in the closed-loop numerator in Eq. (6a) where  $B_{xd'}(s)$ ,  $\Delta B_{xk}(s)$ ,  $\Delta B_{xkG}(s)$ ,  $\Delta B_{xkG}(s)$  are functions of spatial variable  $x$ . In view of the above fact, it is possible to impose global damping effect to the closed-loop control system by designing a prototype polynomial  $D(s)$  with prescribed poles and proper damping effects. Selection of closed-loop poles for prototyping polynomial  $D(s)$  is discussed in next section.

### 3. CONTROLLER DESIGN

In the new HVA, the active controller is a discrete-time one implemented in a digital signal processor (DSP) chip. For controller design and stability analysis in the discrete-time domain, it is recommended to transform Eq. (6a) from  $s$ -domain to  $z$ -domain as

$$\frac{V(x, z)}{R(z)} = \frac{-K(z)B_{xd'}(z) + \sqrt{kJ}\omega_a \Delta B_{xk}(z) + G(z)[K(z)\Delta B_{xkG}(z) + \sqrt{kJ}\omega_a \Delta B_{xkG}(z)]}{K(z)A(z) + \sqrt{kJ}\omega_a B_{p'p'}(z) + G(z)[K(z)B_{pa'}(z) + \sqrt{kJ}\omega_a \Delta B_{kG}(z)]} \quad (7)$$

For better focus on the discussions, one may introduce  $Q(z) = K(z)A(z) + \sqrt{kJ}\omega_a B_{p'p'}(z)$ ,  $M(z) = K(z)B_{pa'}(z) + \sqrt{kJ}\omega_a \Delta B_{kG}(z)$  and re-write Eq. (7) in the following way

$$\frac{V(x, z)}{R(z)} = \frac{-K(z)B_{xd'}(z) + \sqrt{kJ}\omega_a \Delta B_{xk}(z) + G(z)[K(z)\Delta B_{xkG}(z) + \sqrt{kJ}\omega_a \Delta B_{xkG}(z)]}{Q(z) + G(z)M(z)} \quad (8a)$$

$$\text{and} \quad D(z) = Q(z) + G(z)M(z) \quad (8b)$$

such that the closed-loop denominator looks simpler. The secondary path transfer function (open loop transfer function from actuator to feedback sensor) may be non-minimum phase if the actuator is not collocated with the feedback sensor. That may be a reason for most researchers to favor the bundled structure when integrating active control with a passive absorber like Fig. 1b and Fig. 2b (Tso et al., 2013). The pole-placement controller is able to deal with non-minimum phase secondary path transfer functions, and allow a designer more flexibility to choose a better location for the actuator than collocating with the passive part. Parameter polynomials  $Q(z)$  and  $M(z)$  play important roles in the closed-loop denominator. They can be identified with sufficient accuracy via off-line system identification (Hsia, 1977). One may be interested in the sensitivity of a closed-loop transfer function with respect to some degrees of parameter uncertainties or identified model errors. Controller design and its response based on model with parameter uncertainties were thoroughly discussed in one of the co-author's technical report (Yuan, 2004) and will not discuss in this paper.

The controller transfer function  $G(z)$  is a rational function with numerator and denominator polynomials

$$G(z) = \frac{P(z)}{U(z)} \quad (9)$$

where  $P(z) = \sum_{i=0}^{n-1} p_i z^{-i}$ ,  $U(z) = 1 + \sum_{i=1}^{n-1} u_i z^{-i}$ , and  $n$  is the order of the secondary control path transfer function. Substituting Eq. (9) into Eq. (8a), the closed-loop transfer function from disturbance to any points of the primary structure becomes

$$\frac{V(x, z)}{R(z)} = \frac{U(z)[-K(z)B_{xd'}(z) + \sqrt{kJ}\omega_a \Delta B_{xk}(z)] + P(z)[K(z)\Delta B_{xkG}(z) + \sqrt{kJ}\omega_a \Delta B_{xkG}(z)]}{U(z)Q(z) + P(z)M(z)} \quad (10)$$

In Eq. (10), the closed-loop denominator is modified by numerator  $P(z)$  and denominator  $U(z)$  of the controller transfer function  $G(z)$ . One may select a prototype polynomial  $W(z) = 1 + \sum_{i=1}^{2n-1} w_i z^{-i}$  with stable poles and imposed it to the denominator of Eq. (10) such that a Bezout equation is satisfied

$$W(z) = U(z)Q(z) + P(z)M(z). \quad (11)$$

Since  $K(z)$ ,  $A(z)$ ,  $B_{p'p'}(z)$ ,  $B_{pa'}(z)$  and  $\Delta B_{kG}(z)$  are independent of spatial variable  $x$ , polynomials  $Q(z) = K(z)A(z) + \sqrt{kJ}\omega_a B_{p'p'}(z)$  and  $M(z) = K(z)B_{pa'}(z) + \sqrt{kJ}\omega_a \Delta B_{kG}(z)$  are independent of spatial variable  $x$ . Therefore  $W(z)$  is independent of spatial variable  $x$ . The pole placement controller can introduce damping effect to all the positions of the primary structure (instead of a single control point) by assigning closed-loop poles with proper damping effect to the closed-loop characteristic equation. Active damping can be achieved by placing closed-loop poles at desired positions within a unit circle. It is free from any negative effects arising from non-minimum phase secondary control path.

The control objective is to introduce damping effect to whole primary structure for control of global vibration. While the active controller  $G(z)$  is turned on, it matches a prototype polynomial  $W(z)$  to the closed-loop denominator of the control system shown in Eq. (10), and hence making the denominator to possess the desired properties granted by the user. Therefore, it is critically important to choose the roots (or closed-loop poles) of the prototype polynomial  $W(z)$ . In digital control theory (Ogata, 2001), a discrete-time system is stable if all poles are inside a unit circle centered at the origin of the complex plane. The closer its poles to the origin of the complex plane, the faster its impulse response converges. Smaller magnitudes of poles imply heavier damping. Selection of prototype polynomial  $W(z)$  is based on the principle described in (Tso et al., 2013).

In the detached HVA, the feedback sensor may be placed at a proper location such that all vibration modes are observable. For a cantilever beam, the best location of a translational feedback sensor is the free-end point with maximum displacements for all modes. The passive resonator may be mounted at the location where vibration suppression is mostly desirable. In the case of cantilever beam, the best location is also the free end as all modal responses are maximized here. Generally speaking, a passive resonator with weak damping ratio (such as pendulum-like device in the derived model) can create a significant suppression dip at its pre-tuned frequency at the local coupling location but at the expense of inducing two extra sandwich high peaks along the whole coupled structure. With the help of the proposed pole placement controller, active damping can be introduced to the coupling system through prescribed prototype polynomial  $W(z)$  at Eq. (11) and damped down



all remaining peaks at any locations of the coupled structure. This control strategy can keep the desired dip at the interested attenuation location created by the passive resonator as well. The actuator may be attached to the primary structure at a proper location such that all modal dynamics are controllable by the actuator. The rule of thumb is to avoid selecting nodal points of spatial derivative of the  $i^{\text{th}}$  eigen-function of the primary structure such as  $\varphi_i'(x_a) = 0$  since all the spatial derivative of eigen-functions at the actuating point are multiplied with the active control moment  $\tau_a(t)$  as shown in Eq. (A1). Active control element will be ineffective or even incapable to damp down corresponding peaks in case of attaching an actuator to any of the captioned nodal points. Once the mounting location of the passive resonator confirmed, one may choose the best location of the actuator,  $x_a^*$ , by calculating the minimum spatial average mean square response,  $\sigma_{x_a^*}$ , of the coupled structure.

$$\sigma_{x_a^*} = \min \left( \frac{1}{2\pi L} \int_{-\infty}^{+\infty} \int_0^L \left| \frac{V(x,s)}{R(s)} \right|^2 dx d\omega \right); \quad 0 < x_a^* \leq L \quad (12)$$

Practically, this approach offers more flexibility to engineers on selecting locations of actuators or sensors in real applications.

It may be difficult to minimize vibration response at multiple points (equivalent to minimize multiple sets of  $H_2$  or  $H_\infty$  norms of multiple local transfer functions corresponding to multiple points) with a single actuator. However, it is possible to implement the pole placement controller to damp global structural vibration since the closed-loop denominator is the same for all closed-loop transfer functions from the disturbance to different position  $x$ . The controller introduces damping effect to the entire primary structure by assigning one set of closed-loop poles to the closed-loop denominator to achieve the goal of global structural vibration control. In the literature, there are many reports of the bundled HVA for single-point structural vibration control. However, there are few reports on the feasibility of implementing a HVA with a single feedback sensor for structural vibration control of multiple points over a wide band frequency excitation. In this study, our objective is to design a detached HVA for global structural vibration control over a wide frequency band. To the best of Authors' knowledge, this is the first report to address such kind of control approach and absorber design in the literature.

#### 4. EXPERIMENTAL SETUP

The active controller and detached HVA were verified by experimental results. The controller was implemented in a dSpace rapid prototype controller board – ds1104 (integrated with A/D and D/A converters). All analog signals were filtered by the Alligator anti-alias filter board – AAF-3PCI (with AAF-3F modules) before being sampled into the digital system. The feedback sensor was a Brüel & Kjær Accelerometer – type 4374; and the monitor sensor was a Picomin Accelerometer – model 22. The acceleration signals were amplified by a Brüel & Kjær 4-channel NEXUX charge conditioning amplifier – type 2692 (with double integration function). The actuator was a Noliac Piezoelectric bender – CMBP06. It was driven by a Noliac 1-channel voltage amplifier – NDR 6110.

The secondary path transfer function,  $\frac{V_p(z)}{T_a(z)} = \frac{M(z)}{Q(z)}$ , is available from off-line system

identification. Roots of  $Q(z)$  and  $M(z)$  can be modified and damped down by the pole placement controller. One may apply a signal generator to generate pseudo white noise as the input to the secondary control path and collect the output signals via one or more monitor sensors placed at different points. The number of output channels equals to the number of transfer functions to be identified. In the experimental study, only the secondary path transfer function from the actuator to the feedback accelerometer is identified and the output channel number is one. It is important to place the actuator at a proper point on the primary structure such that all modal dynamics are controllable by the actuator. It is also important to place the feedback sensor at proper point such that all vibration modes are fully observable by the sensor. In our experiments, the feedback accelerometer is attached at the free-end of the primary structure from which all vibration modes are observable. Such a configuration avoids possible common roots shared by polynomials  $Q(z)$  and  $M(z)$  to ensure that the Sylvester resultant in Eq. (11) would be non-singular.

The sampling frequency of the control system was set to  $1720\text{Hz}$  and the cut-off frequency of the anti-aliasing filter was tuned to  $600\text{Hz}$ . In the experiment, the maximum frequency of interest was  $520\text{Hz}$  which is reasonably less than the anti-aliasing frequency. According to Nyquist sampling theory, the sampling frequency should be at least twice the maximum frequency of interest. In practice, oversampling is necessary in order to cover the transition band of the anti-aliasing filter. The sample size of each experiment was 40,000. The controller is mathematically given by Eq. (9) and was programmed with the help the dSpace ControlDesk. The controller program was compiled via the MatLab Realtime workshop and loaded into the dSpace ds1104 via the dSpace ControlDesk.

A cantilever beam shown in Fig. 2a was used in the experiments as the primary structure. Its dimensions are  $150\text{mm}$  (length)  $\times$   $30\text{mm}$  (width)  $\times$   $3\text{mm}$  (thickness) with a weight of  $0.095\text{kg}$  and fabricated with mild steel. The stainless steel absorber, which is actually a distributed mass system, has dimensions of  $85\text{mm}$  (length)  $\times$   $20\text{mm}$  (width)  $\times$   $1\text{mm}$  (thickness) with a weight of  $0.015\text{kg}$  or a mass ratio of 15.8%. The passive resonance was tuned to the first resonant peak of the primary structure by adjusting the position of the screw-washer-nut set in the slot of the absorber. The passive part of the detached HVA was mounted at the free-end of the primary cantilever beam while its active element, a piezoelectric bender, was attached on the primary structure at position  $x=25\text{mm}$ . Both coupling locations of passive DVA and active element were not nodal points to ensure that all vibration modes were fully controllable. As space was limited in the small scale of the primary cantilever beam, the active element of the absorber was also used as the disturbance source in the experiments. Practically, it is not necessarily to add an extra actuator as the disturbance source since disturbance may excite the primary structure at any positions in real applications.

In Eq. (11), the prototype polynomial  $W(z)$  and parameter polynomials  $Q(z)$  and  $M(z)$  of the secondary path transfer function are all independent of polynomial  $B_{xd}$ . That means location of the disturbance would not affect the performance of the pole-placement controller. An accelerometer was used as feedback sensor and mounted at the free-end of the primary cantilever beam in Fig. 1a to ensure that all vibration modes were fully observable. Another accelerometer sensor was used as a monitor sensor to measure the structural linear velocity response at five more different locations as shown in Fig. 1a. Measurements of the monitor sensor were collected sequentially at multiple points to evaluate performance of the detached HVA. Signals from both accelerometers were integrated by the 4-channel charge conditioning amplifier to obtain linear velocity signals for control and monitor purpose. The dSpace ds1104 controller board was used to capture monitor sensor signals for further analysis, to generate white noise signals and to synthesize control signals for the piezoelectric bender.

In the experiments, three sets of experimental data were collected to compare the performance of the proposed hybrid absorber under three different control conditions. Those conditions were (i) primary beam structure without any control (raw beam), (ii) primary structure with passive control by switching off the active controller and (iii) primary structure with the proposed HVA control by switching on the controller. Under each of the experiment conditions, transversal linear velocities of the beam was measured with a monitor sensor sequentially at  $x=50\text{mm}$ ,  $70\text{mm}$ ,  $90\text{mm}$ ,  $110\text{mm}$ ,  $130\text{mm}$  and  $150\text{mm}$  as shown in Fig. 1a. That means six sub-sets of monitor data were collected under each experiment condition. Each sub-set contains two sequences  $\{r(1) \ r(2) \ \dots \ r(N)\}$  and

$\{v_x(1) \ v_x(2) \ \dots \ v_x(N)\}$  with the same sample size of  $N=40,000$  where the first sequence is white noise disturbance signals and the second one is the linear velocity signals measured at  $x = 50mm, 70mm, 90mm, 110mm, 130mm$  and  $150mm$ . The captured signals were transformed to the frequency domain using MatLAB command “pwelch” and then plotted as the normalized power spectral densities (PSDs)  $\left| \frac{V(e^{-j\omega\delta T}, x)}{R(e^{-j\omega\delta T})} \right|$  (in dB scale) with  $\delta T$  denoted as the sampling time. The frequency response can be used to visualize the control performance of the passive absorber or hybrid vibration absorber on structural vibration at multiple monitor points.

## 5. EXPERIMENTAL AND SIMULATION RESULTS

A passive dynamic vibration absorber was used to compare with the detached hybrid vibration absorber on their suppression performance over global structural vibration. The difference between passive and hybrid absorber is only switching off and on the active controller. Frequency responses of position  $x$ , for  $x=150mm, 90mm$  and  $50mm$  were measured and plotted in Figs. 3, 4 and 5 respectively. These responses reveal the respective attenuation performance of the two control devices on structural vibration at multiple monitor locations of the primary structure.

Figure 3 plots power spectrum densities (PSD's) of the velocity signal subject to three respective conditions: (i) a raw beam without vibration control, (ii) vibration control with passive resonator and (iii) vibration control with the detached HVA all measured at  $x=150 \text{ mm}$ . The resonant frequency of the passive resonator was tuned to 78 Hz to match the first resonant peak of the raw beam. When coupled with the beam, the passive resonator caused an attenuation dip over 40 dB at 78 Hz and also suppressed the second resonant peak (at 520 Hz) of the raw beam. As a side effect, the resonator pushed the first resonant peak of the raw beam at one side and introduced an extra peak at another side in the frequency domain. The two strong peaks sandwiched the attenuation dip, which is typical drawback of passive absorbers. These peaks were stronger than the first resonant peak of the raw beam. Generally, a passive resonator introduces attenuation to the primary structure at a pre-tuned frequency, however, such attenuation is only effective at the coupling point of the resonator and have no effects to other locations of the primary structure (refer to Figs. 4 and 5). Besides, the attenuation level is directly linked to the damping ratio of the passive resonator. A resonator with weaker damping ratio can introduce deeper attenuation to the primary structure at the expense of stronger peaks at other frequencies. Therefore, trade-off between keeping a deep attenuation dip (with weak damping ratio) and reducing all peaks (with stronger damping ratio) is a

dilemma faced by designers of passive absorbers. The control performance of the detached HVA is plotted as the black and thick solid curve. One can see that the attenuation dip of the passive resonator can still be kept by active control while the first two peaks of the coupled system can be damped down effectively. That is one of the features of the detached HVA. Active damping can be introduced to suppress the vibration peaks without affecting the attenuation dip. Users can tune the attenuation dip to the desired frequency by adjusting the frequency of passive resonator. Experimental results show that the extra peak caused by the passive resonator can be damped down by over 20 dB.

Figure 4 presents the control performance of the passive resonator and the detached HVA on structural vibration at position  $x=90mm$ . The passive resonator attenuated the first two resonance peaks of the raw beam but introduced an extra peak, making a total of four peaks in the frequency range of interest. Similar to Fig. 3, the first peak in the coupled system was as strong as the first peak of the raw beam. The other three peaks of the coupled system were weaker but no attenuation dip in the frequency range of interest. Similarly, the detached HVA can damp down all the peaks, with the first peak damped down by as much as 20 dB.

Figure 5 demonstrates the control performance of passive resonator and the detached HVA at a location far away from the coupling point ( $x=50mm$ ). The passive resonator can attenuate the first two resonant peaks of the raw beam at the expense of an extra peak, with the first peak of the coupled system 10 dB higher than the first peak of the raw beam. When the detached HVA was turned on, the first two peaks of the coupled system were damped down by as much as 30 dB. A possible reason may be that location  $x=50mm$  was very close to the actuator attached at  $x=25mm$ . The actuator was more effective attenuating vibration at this point than at the other two monitor points  $x=150mm$  and  $90mm$  respectively.

From the experimental results and the above observations, one can see that the detached HVA provides excellent attenuation effect to the peaks of the coupled system at multiple points of the primary structure. It is able to keep the attenuation dip of the passive absorber while introducing active damping to the primary structure for vibration suppression.

Experimental results of the detached HVA *are* compared with experimental data of the bundled HVA (Tso et al., 2013). Mean square velocity,  $P_x = \left( \frac{1}{N} \right) \sum_{i=1}^N v_x^2(i)$ , of the beam structure measured at  $x = 150mm, 130mm, 110mm, 90mm, 70mm, 50mm$  and the spatial average value were plotted in Fig. 6. The beam structure were under three cases of control condition such as (i) raw beam without

control (black bar), (ii) control with proposed detached HVA (gray bar) and (iii) control with bundled HVA (white bar). Fig. 6 showed that the values of mean square velocity of the detached HVA were generally smaller than the bundled HVA at all monitor positions except at the tip of the primary structure. This is because the tip position was the coupling point of the bundled HVA, so the attenuation performance of the bundled HVA was more effective than the detached HVA. However, the suppression power of the bundled HVA was gradually weakened with monitor locations far away from its coupling point such as  $x = 70mm$  and  $50mm$ . While observing the detached HVA, it was found that the detached HVA can mitigate structural vibration effectively on all monitor positions and hence the detached HVA has a smaller spatial average value than the bundled HVA. The reason is as the passive resonator and active actuator were mounted respectively at the tip and a point with rigid support nearby, the mitigation power on structural vibration can distribute evenly along the whole structure. This superiority demonstrates the merit of the detached design of the proposed detached HVA.

Simulations were also conducted to compare the detached HVA with the bundled HVA when both were applied to suppress vibration of a cantilever beam. All boundary conditions and external disturbance were the same in the simulation. The only difference was locations of the actuators used in the simulation. Passive resonators of the HVA's were located at  $x_p=L$ . The feedback and monitor sensors were the same in the simulations at  $x_m=L$ . The only difference was actuator location with  $x_a=0.143L$  for the detached HVA and  $x_a=L$  for the bundled HVA. The numerical simulation results were calculated based on Eqs. (6a) and (6b) as closed-loop transfer function from disturbances to any point  $x$  of the primary structure under control of the detached HVA. Detailed derivations of Eqs. (6a) and (6b) are given in the appendix. Calculation formulations of the bundled HVAs are shown in the appendix of authors' previous paper (Tso et al., 2013) and the respective numerical results were calculated based on Eq. (A13). The damped poles of the closed-loop denominator used in the simulation were selected based on Eq. (21) of the authors' another paper (Tso et al., 2012). A-plot was generated from the simulation results and shown in Fig. 7. The detached HVA was able to damp down vibration in a wider frequency range than the bundled HVA, as shown in Fig. 7.

Simulation and experimental results of the detached HVA with respect to Fig. 7 and Fig. 3 were compared. Both results show the significant attenuation dip created by the passive resonator can be kept at the tip position of the primary structure while all resonant peaks of the couple system are damped down by the active controller. The proposed detached HVA was verified both theoretically and experimentally to demonstrate its excellent performance on global vibration control within a broadband frequency.

To select the actuator location, one may use the spatial average mean square response,

$$\frac{1}{2\pi L} \int_{-\infty}^{+\infty} \int_0^L \left| \frac{V(e^{-j\omega\delta T}, x)}{R(e^{-j\omega\delta T})} \right|^2 dx d\omega, \text{ of the primary structure under detached HVA control as an objective}$$

function. This is the function of actuator location in our simulation and plotted in Fig. 8. The actuating location was the spatial variable along the primary structure with length  $L$  such as  $0 < x_a \leq L$ . The primary structure was equally separated with 1000 intervals. The passive resonator and sensor were mounted at the tip position of a cantilever beam at the beginning. A minimum value of spatial average mean square response was achieved when the actuator was mounted at approximate  $0.143L$ . This is the optimal location of the actuator in the numerical simulation. A number of peaks corresponding to different locations of actuating point were found in Fig. 8 as well. The objective function reached those peaks because the actuator was located at the nodal points of spatial derivative of eigen-functions or at the vicinity of these points. For example, the high peaks located at approximate  $0.2L$  and  $0.29L$  is respectively near the nodal points of the spatial derivative of the 4<sup>th</sup> and 3<sup>rd</sup> eigen-functions.

## 6. CONCLUSIONS

A new HVA with detached active and passive control elements is proposed as an alternative design to the traditional bundled HVA with collocated active and passive control elements for vibration suppression of dynamic structures. HVA is effective in controlling structural vibration of cantilever like structures such as buildings and towers. However, space or loading limits may impose restrictions on the applications of the traditional bundled HVA. The proposed HVA with detached elements provides engineers with more flexibility to retrofit a passive DVA into a high performance HVA by installing the actuator at a more suitable location. In this study, active part of the new HVA is regulated by a pole placement controller. It is free from any negative effects arising from possibly non-minimum phase secondary path due to non-collocation or mismatch of actuator-sensor pairs. This *feature does* not exist in a bundled HVA with collocated actuator-sensor pairs. The detached HVA and active controller are analyzed thoroughly in this paper. Experimental and simulation results are used to verify the theoretical controller and demonstrated the excellent performance of the proposed HVA on vibration control of a flexible structure. A traditional bundled HVA is compared with the proposed one using previously available experimental results and in fresh simulations. It is found that the detached HVA can be outperformed the bundled HVA in some applications like the one shown in our experimental and simulation results. A numerical procedure is proposed here to

select the optimal actuator location that is not necessarily the coupling point of the passive resonator. This new finding may lead to a better alternative on HVA design for vibration engineers, one may miss a better solution by neglecting the detached design of HVA.

## **ACKNOWLEDGE**

This project was partially supported by internal grants G-U860 and G-YL55 from the Hong Kong Polytechnic University.



## Appendix A:

Modal decomposition may be applied to Eq. (1) by inner product with the  $i^{th}$  eigen-function to obtain

$$\ddot{\eta}_i(t) + 2\xi_i\omega_i\dot{\eta}_i(t) + \omega_i^2\eta_i(t) = -r(t)\phi'_i(x_d) - \tau_p(t)\phi'_i(x_p) - \tau_a(t)\phi'_i(x_a) \quad i=1,2,3\dots \quad (A1)$$

where  $\xi_i$  and  $\omega_i$  denotes the  $i^{th}$  modal damping ratio and natural frequency of the primary structure respectively.

Let  $H_i(s)$ ,  $R(s)$ ,  $\Phi(s)$  and  $\Theta(s)$  denote the Laplace transforms of  $\eta_i(t)$ ,  $r(t)$ ,  $\phi(t)$  and  $\theta_a(t)$  respectively, one may apply Laplace transform to Eqs. (A1), (2) and (3) to obtain

$$H_i(s) = \frac{-\phi'_i(x_d)R(s) - \phi'_i(x_p)T_p(s) - \phi'_i(x_a)T_a(s)}{s^2 + 2\xi_i\omega_i s + \omega_i^2}, \quad i=1,2,3\dots \quad (A2)$$

$$T_p(s) = k[\Phi(s) - \Theta_p(s)], \quad (A3)$$

$$T_p(s) = -s^2 J\Phi(s) \quad (A4)$$

Substituting Eq. (A4) into Eq. (A3), one may eliminate  $\Phi(s)$  to have

$$T_p(s) = k\left[-\frac{T_p(s)}{s^2 J} - \Theta_p(s)\right] = -\frac{s^2 k}{K(s)}\Theta_p(s) \quad (A5)$$

where  $K(s) = s^2 + \frac{k}{J}$ . One may further substitute Eqs. (A5) and (5) into Eq. (A2) to eliminate  $T_p$  and

$T_a$ . The result is

$$\begin{aligned} H_i(s) &= \frac{-\phi'_{id}K(s)R(s) + s^2 k\phi'_{ip}\Theta_p(s) - G(s)K(s)\phi'_{ia}V_p(s)}{K(s)[s^2 + 2\xi_i\omega_i s + \omega_i^2]} \\ &= \frac{-\phi'_{id}K(s)R(s) + s^2 \sqrt{kJ}\omega_a\phi'_{ip}\Theta_p(s) - G(s)K(s)\phi'_{ia}V_p(s)}{K(s)[s^2 + 2\xi_i\omega_i s + \omega_i^2]} \end{aligned} \quad (A6)$$

where  $\phi'_{id} = \phi'_i(x_d)$ ,  $\phi'_{ip} = \phi'_i(x_p)$  and  $\phi'_{ia} = \phi'_i(x_a)$  for  $i = 1, 2, 3\dots$  and  $k = \sqrt{kJ}\sqrt{\frac{k}{J}} = \sqrt{kJ}\omega_a$

and  $\omega_a$  is the pre-tuned resonance of the passive part of the detached HVA.

Linear velocity of the beam at the sensor location is given in Eq. (4a), with Laplace transform  $V(x, s) = sW(x, s)$ . One may substitute Eq. (A6) into Laplace transform domain of Eq. (4a) to write

$$V_x(s) = sW(x, s) = s \left\{ \sum_{i=1}^{\infty} \phi_{ix} \left\{ \frac{-\phi'_{id}K(s)R(s) + s^2 \sqrt{kJ}\omega_a\phi'_{ip}\Theta_p(s) - G(s)K(s)\phi'_{ia}V_p(s)}{K(s)[s^2 + 2\xi_i\omega_i s + \omega_i^2]} \right\} \right\} \quad (A7a)$$

$$= s \left( \frac{-B_{xd'}(s)K(s)R(s) + s^2 \sqrt{kJ} \omega_a B_{xp'}(s) \Theta_p(s) - G(s)K(s)B_{xa'}(s)V_p(s)}{K(s)A(s)} \right)$$

where  $\varphi_{ix} = \varphi_i(x)$ ,

$$A(s) = \prod_{i=1}^{\infty} (s^2 + 2\xi_i \omega_i s + \omega_i^2), \quad (\text{A7b})$$

$$B_{xd'}(s) = \sum_{i=1}^{\infty} \left\{ \varphi_{ix} \varphi'_{id} \left[ \prod_{k \neq i} (s^2 + 2\xi_k \omega_k s + \omega_k^2) \right] \right\}, \quad (\text{A7c})$$

$$B_{xp'}(s) = \sum_{i=1}^{\infty} \left\{ \varphi_{ix} \varphi'_{ip} \left[ \prod_{k \neq i} (s^2 + 2\xi_k \omega_k s + \omega_k^2) \right] \right\}, \quad (\text{A7d})$$

$$B_{xa'}(s) = \sum_{i=1}^{\infty} \left\{ \varphi_{ix} \varphi'_{ia} \left[ \prod_{k \neq i} (s^2 + 2\xi_k \omega_k s + \omega_k^2) \right] \right\}. \quad (\text{A7e})$$

Angular displacement of the beam at the sensor location is given in Eq. (4b), with Laplace transform  $\Theta(x_p, s)$ . One may substitute Eq. (A6) into Laplace transform domain of Eq. (4b) to write

$$\begin{aligned} \Theta_p(s) &= \Theta(x_p, s) = - \sum_{i=1}^{\infty} \varphi'_{ip} \left\{ \frac{-\varphi'_{id} K(s)R(s) + s^2 \sqrt{kJ} \omega_a \varphi'_{ip} \Theta_p(s) - G(s)K(s) \varphi'_{ia} V_p(s)}{K(s)[s^2 + 2\xi_i \omega_i s + \omega_i^2]} \right\} \\ &= \frac{B_{p'd'}(s)K(s)R(s) - s^2 \sqrt{kJ} \omega_a B_{p'p'}(s) \Theta_p(s) + G(s)K(s)B_{p'a'}(s)V_p(s)}{K(s)A(s)} \\ &= \frac{B_{p'd'}(s)K(s)R(s) + G(s)K(s)B_{p'a'}(s)V_p(s)}{K(s)A(s) + s^2 \sqrt{kJ} \omega_a B_{p'p'}(s)} = P_{\theta_r}(s)R(s) + P_{\theta_v}(s)V_p(s) \end{aligned} \quad (\text{A8a})$$

where

$$B_{p'd'}(s) = \sum_{i=1}^{\infty} \left\{ \varphi'_{ip} \varphi'_{id} \left[ \prod_{k \neq i} (s^2 + 2\xi_k \omega_k s + \omega_k^2) \right] \right\}, \quad (\text{A8b})$$

$$B_{p'p'}(s) = \sum_{i=1}^{\infty} \left\{ \varphi'_{ip} \varphi'_{ip} \left[ \prod_{k \neq i} (s^2 + 2\xi_k \omega_k s + \omega_k^2) \right] \right\}, \quad (\text{A8c})$$

$$B_{p'a'}(s) = \sum_{i=1}^{\infty} \left\{ \varphi'_{ip} \varphi'_{ia} \left[ \prod_{k \neq i} (s^2 + 2\xi_k \omega_k s + \omega_k^2) \right] \right\}, \quad (\text{A8d})$$

$$P_{\theta_r}(s) = \frac{B_{p'd'}(s)K(s)}{K(s)A(s) + s^2 \sqrt{kJ} \omega_a B_{p'p'}(s)}, \quad (\text{A8e})$$

$$P_{\theta_v}(s) = \frac{G(s)B_{p'a'}(s)K(s)}{K(s)A(s) + s^2 \sqrt{kJ} \omega_a B_{p'p'}(s)}, \quad (\text{A8f})$$

For the linear velocity of the beam, at the sensor location  $V(x, s) = sW(x, s)$ , one may focus on the feedback sensor location by substituting  $x=x_p$  into Eq. (A7) to write

$$\begin{aligned}
V_p(s) &= s \left\{ \sum_{i=1}^{\infty} \varphi_{ip} \left\{ \frac{-\varphi'_{id} K(s) R(s) + s^2 \sqrt{kJ} \omega_a \varphi'_{ip} \Theta_p(s) - G(s) K(s) \varphi'_{ia} V_p(s)}{K(s) [s^2 + 2\xi_i \omega_i s + \omega_i^2]} \right\} \right\} \\
&= s \left( \frac{-B_{pd'}(s) K(s) R(s) + s^2 \sqrt{kJ} \omega_a B_{pp'}(s) \Theta_p(s) - G(s) K(s) B_{pa'}(s) V_p(s)}{K(s) A(s)} \right) \\
&= \frac{-s B_{pd'}(s) K(s) R(s) + s^3 \sqrt{kJ} \omega_a B_{pp'}(s) \Theta_p(s)}{K(s) A(s) + s G(s) K(s) B_{pa'}(s)} = P_{vr}(s) R(s) + P_{v\theta}(s) \Theta_p(s), \tag{A9a}
\end{aligned}$$

where  $\varphi_{ip} = \varphi_i(x_p)$ ,

$$B_{pd'}(s) = \sum_{i=1}^{\infty} \left\{ \varphi_{ip} \varphi'_{id} \left[ \prod_{k \neq i} (s^2 + 2\xi_k \omega_k s + \omega_k^2) \right] \right\}, \tag{A9b}$$

$$B_{pp'}(s) = \sum_{i=1}^{\infty} \left\{ \varphi_{ip} \varphi'_{ip} \left[ \prod_{k \neq i} (s^2 + 2\xi_k \omega_k s + \omega_k^2) \right] \right\}, \tag{A9c}$$

$$B_{pa'}(s) = \sum_{i=1}^{\infty} \left\{ \varphi_{ip} \varphi'_{ia} \left[ \prod_{k \neq i} (s^2 + 2\xi_k \omega_k s + \omega_k^2) \right] \right\}. \tag{A9d}$$

$$P_{vr}(s) = \frac{-s B_{pd'}(s) K(s)}{K(s) [A(s) + s G(s) B_{pa'}(s)]}, \tag{A9e}$$

$$P_{v\theta}(s) = \frac{s^3 \sqrt{kJ} \omega_a B_{pp'}(s)}{K(s) [A(s) + s G(s) B_{pa'}(s)]}, \tag{A9f}$$

One may substitute Eqs. (A8a) into (A7a) to obtain

$$\Theta_p(s) = P_{\theta r}(s) R(s) + P_{\theta v}(s) [P_{vr}(s) R(s) + P_{v\theta}(s) \Theta_p(s)]$$

which is equivalent to

$$\Theta_p(s) = \frac{P_{\theta r}(s) + P_{\theta v}(s) P_{vr}(s)}{1 - P_{\theta v}(s) P_{v\theta}(s)} R(s). \tag{A10}$$

After substituting Eqs. (A8e), (A8f), (A9e) and (A9f), one obtains

$$\Theta_p(s) = \frac{K(s) B_{p'd'}(s) + s K(s) G(s) \Delta B_{kG}(s)}{[K(s) A(s) + s G(s) K(s) B_{pa'}(s) + s^2 \sqrt{kJ} \omega_a B_{pp'}(s)] + s^3 \sqrt{kJ} \omega_a G(s) \Delta B_{kG}(s)} R(s) \tag{A11a}$$

where

$$\Delta B_{kG}(s) = B_{pa'}(s) B_{p'p'}(s) - B_{p'a'}(s) B_{pp'}(s), \tag{A11b}$$

$$\Delta B_{KG}(s) = B_{pa'}(s) B_{p'd'}(s) - B_{p'a'}(s) B_{pd'}(s). \tag{A11c}$$

The next step is to eliminate  $\Theta_p(s)$  by substituting Eqs. (A8a) into (A9a) to obtain

$$V_p(s) = P_{vr}(s) R(s) + P_{v\theta}(s) [P_{\theta r}(s) R(s) + P_{\theta v}(s) V_p(s)]$$

which is equivalent to

$$V_p(s) = \frac{P_{vr}(s) + P_{v\theta}(s)P_{\theta r}(s)}{1 - P_{v\theta}(s)P_{\theta v}(s)} R(s). \quad (\text{A12})$$

After substituting Eqs. (A8e), (A8f), (A9e) and (A9f), one obtains

$$V_p(s) = \frac{-sK(s)B_{pd'}(s) + s^3\sqrt{kJ}\omega_a\Delta B_k(s)}{[K(s)A(s) + sG(s)K(s)B_{pa'}(s) + s^2\sqrt{kJ}\omega_a B_{p'p'}(s)] + s^3\sqrt{kJ}\omega_a G(s)\Delta B_{kG}(s)} R(s) \quad (\text{A13a})$$

where

$$\Delta B_k(s) = B_{pp'}(s)B_{p'd'}(s) - B_{pd'}(s)B_{p'p'}(s). \quad (\text{A13b})$$

At any location, linear velocity of the beam can be obtained by substituting Eqs. (A10) and (A12) into Eq. (8a). The result is

$$\begin{aligned} V(x,s) &= \frac{s}{K(s)A(s)} \left\{ -B_{xd'}(s)K(s)R(s) + s^2\sqrt{kJ}\omega_a B_{xp'}(s)\Theta_p(s) - G(s)K(s)B_{xa'}(s)V_p(s) \right\} \\ &= \left\{ -\frac{sB_{xd'}(s)}{A(s)} + \frac{s^3\sqrt{kJ}\omega_a B_{xp'}(s)[P_{\theta r}(s) + P_{\theta v}(s)P_{vr}(s)]}{K(s)A(s)[1 - P_{\theta v}(s)P_{v\theta}(s)]} - \frac{sG(s)B_{xa'}(s)[P_{vr}(s) + P_{v\theta}(s)P_{\theta r}(s)]}{A(s)[1 - P_{v\theta}(s)P_{\theta v}(s)]} \right\} R(s) \end{aligned}$$

which is equivalent to

$$\begin{aligned} \frac{V(x,s)}{R(s)} &= \frac{-sK(s)B_{xd'}(s) + s^2K(s)G(s)\Delta B_{xKG}(s) + s^3\sqrt{kJ}\omega_a\Delta B_{xk}(s) + s^4\sqrt{kJ}\omega_a G(s)\Delta B_{xkG}(s)}{[K(s)A(s) + sG(s)K(s)B_{pa'}(s) + s^2\sqrt{kJ}\omega_a B_{p'p'}(s)] + s^3\sqrt{kJ}\omega_a G(s)\Delta B_{kG}(s)} \\ &= \frac{-sK(s)B_{xd'}(s) + s^3\sqrt{kJ}\omega_a\Delta B_{xk}(s) + G(s)[s^2K(s)\Delta B_{xKG}(s) + s^4\sqrt{kJ}\omega_a\Delta B_{xkG}(s)]}{K(s)A(s) + s^2\sqrt{kJ}\omega_a B_{p'p'}(s) + G(s)[sK(s)B_{pa'}(s) + s^3\sqrt{kJ}\omega_a\Delta B_{kG}(s)]} \quad (\text{A14a}) \end{aligned}$$

after substituting Eqs. (A8e), (A8f), (A9e) and (A9f). This is the closed-loop transfer function from disturbance  $R(s)$  to any measurement location  $x$  on the primary structure, where

$$\Delta B_{xKG}(s) = B_{xa'}(s)B_{pd'}(s) - B_{xd'}(s)B_{pa'}(s), \quad (\text{A14b})$$

$$\Delta B_{xk}(s) = B_{xp'}(s)B_{p'd'}(s) - B_{xd'}(s)B_{p'p'}(s). \quad (\text{A14c})$$

References:

- Balas MJ (1978) Active control of flexible systems. *Journal of Optimization Theory and Applications* 25 415-436.
- Banks HT, Luo Z-H, Bergman LA and Inman DJ (1998) On the Existence of Normal Modes of Damped Discrete-Continuous Systems. *Journal of Applied Mechanics* 65 980-989.
- Cha PD and Zhou X (2006) Imposing points of zero displacements and zero slopes along any linear structure during harmonic excitations. *Journal of Sound and Vibration* 297 55-71.
- Chang JCH and Soong TT (1980) Structural control using active tuned mass dampers. *Journal of the Engineering Mechanics Division, ASCE* 1061091-1098.
- Chen XZ, Kareem A (2004) Equivalent static wind loads on buildings: new model. *Journal of Structural Engineering* 130 1425-1435.
- Chen YD, Fuh CC and Tung PC (2005) Application of voice coil motors in active dynamic vibration absorbers. *IEEE Transactions on Magnetics* 41 1149-1154.
- Cheung YL and Wong WO (2008) Isolation of bending vibration in a beam structure with a translational vibration absorber and a rotational vibration absorber. *Journal of Vibration and Control* 14 1231-1246.
- Cheung YL and Wong WO (2009)  $H_\infty$  and  $H_2$  optimizations of a dynamic vibration absorber for suppressing vibrations in plates. *Journal of Sound and Vibration* 320 29-42.
- Daley S and Wang J (2008) A geometric approach to the design of remotely located vibration control systems. *Journal of Sound and Vibration* 318 702-714.
- Dayou J and Brennan MJ (2002) Global control of structural vibration using multiple-tuned tunable vibration neutralizers. *Journal of Sound and Vibration* 258 345-357.
- Fujita T, Kamada T and Masaki N (1993) Fundamental study of active mass damper using multistage rubber bearing and hydraulic actuator for vibration control of tall buildings (2nd report, excitation tests for experimental model of building with mass damper). *Transactions of the Japan Society of Mechanical Engineers, Part C* 59 71-77.
- Hermann F (1909) Device for damping vibrations of bridges. German Patent 525455.
- Hsia TC (1977) *System Identification: Least-Square Methods*. Toronto: Lexington.
- Inman DJ (1994) *Engineering vibrations*. Prentice-Hill, NJ.

Jacquot RG (2003) The spatial average mean square motion as an objective function for optimizing damping in damped modified systems. *Journal of Sound and Vibration* 259 955-965.

Kosut RL (1970) Suboptimal control of linear time-invariant systems subject to control structure constraints. *IEEE Transactions on Automatic Control* 15 557-563.

Kumagai T, Hashimoto R, Wada M, Tanaka M, and Yoshida Y (1993) Control of an active mass damper using a neural network. *Transactions of the Japan Society of Mechanical Engineers, Part C* 59 2305-2311.

Lesieutre GA, Rusovici R, Koopmann GH and Dosch JJ (2003) Modelling and characterization of a piezoceramic inertial actuator. *Journal of Sound and Vibration* 261 93-107.

Nishimura H, Yoshida K and Shimogo T (1989) Optimal Dynamic Vibration Absorber for Multi-Degree-of-Freedom Systems : Theoretical Consideration in the Case of Random Input. *JSME International Journal. Ser. 3, Vibration, Control Engineering, Engineering for Industry* 32 373-379.

Nonami K, Nishimura H and Tian H (1996)  $H_\infty / \mu$  control-based frequency-shaped sliding mode control for flexible structures. *JSME international journal. Ser. C, Dynamics, control, robotics, design and manufacturing* 39 493-501.

Ogata K (2001) *Modern Control Engineering*. NJ: Prentice Hall.

Olgac N and Holm Hansen BT (1994) A novel active vibration absorption technique: delayed resonator. *Journal of Sound and Vibration* 176 93-104.

RA Burdisso and Heilmann JD (1998) A new dual-reaction mass dynamic vibration absorber actuator for active vibration control. *Journal of Sound and Vibration* 214 817-831.

Solari G (1988) Equivalent wind spectrum technique: theory and applications. *Journal of Structural Engineering* 114 1303-1323.

Sun JQ, Jolly MR and Norris MA (1995) Passive, adaptive and active tuned vibration absorbers---a survey. *Journal of Mechanical Design* 117 234-242.

Tso MH, Yuan J, and Wong WO (2012) Suppression of random vibration in flexible structures using a hybrid vibration absorber. *Journal of Sound and Vibration* 331 974-986.

Tso MH, Yuan J, and Wong WO (2013) Design and experimental study of a hybrid vibration absorber for global vibration control. *Engineering structures* 56 1058-1069.

Watanabe T and Yoshida K (1994) Evaluation and Optimization of Parallel Hybrid Active Dynamic Vibration Absorbers. *JSME International Journal. Ser. C, Dynamics, Control, Robotics, Design and Manufacturing* 37 471-476.

Yuan J (2000) Hybrid vibration absorption by zero/pole-assignment. *Journal of Vibration and Acoustics* 122 466-469.

Yuan J (2001) Multi-point hybrid vibration absorption in flexible structures. *Journal of Sound and Vibration* 241 797-807.

Yuan J (2004) Global damping of a vibration structure with a locally controlled absorber. *AIAA Journal* 42 1802-1805.

**Figure Captions:**

Fig. 1a Cantilever beam and detached HVA with locations of actuator ( $x = x_a$ ), resonator ( $x = x_p$ ), disturbance ( $x = x_d$ ), feedback and monitor sensors.

Fig. 1b Cantilever beam and bundled HVA with collocated actuator and resonator at location ( $x = x_a$ ), disturbance ( $x = x_d$ ), feedback and monitor sensors.

Fig. 2a Experimental rig (a cantilever beam coupled with a detached HVA).

Fig. 2b Experimental rig (a cantilever beam coupled with a bundled hybrid vibration absorber).

Fig. 3 Comparison of PSD,  $\left| \frac{V(e^{-j\omega\delta T}, x)}{R(e^{-j\omega\delta T})} \right|$ , measured at  $x=150mm$  of the primary structure:

..... raw beam; — with passive absorber; — with detached HVA

Fig. 4 Comparison of PSD,  $\left| \frac{V(e^{-j\omega\delta T}, x)}{R(e^{-j\omega\delta T})} \right|$ , measured at  $x=90mm$  of the primary structure:

..... raw beam; — with passive absorber; — with detached HVA

Fig. 5 Comparison of PSD,  $\left| \frac{V(e^{-j\omega\delta T}, x)}{R(e^{-j\omega\delta T})} \right|$ , measured at  $x=50mm$  of the primary structure:

..... raw beam; — with passive absorber; — with detached HVA



Fig. 6 Mean square velocity,  $P_x = \left(\frac{1}{N}\right) \sum_{i=1}^N v_x^2(i)$ , of the beam structure in Fig. 1a measured at  $x=150mm, 130mm, 110mm, 90mm, 70mm, 50mm$  and the spatial average value for the cases of



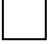
- (i.)  raw beam ( $P_{x\_Beam}$ ),
- (ii.)  Control with proposed “detached hybrid absorber ( $P_{x\_detached\_HVA}$ ) and
- (iii.)  Control with “bundled hybrid absorber ( $P_{x\_bundled\_HVA}$ ).

Fig. 7 Simulated vibration velocity PSD,  $\left| \frac{V(e^{-j\omega\delta T}, x)}{R(e^{-j\omega\delta T})} \right|$ , measured at  $x_m=L$  of the primary structure: - - - - raw beam; — with bundled HVA; — with detached HVA.

Fig. 8 Spatial average mean square response,  $\frac{1}{2\pi L} \int_{-\infty}^{+\infty} \int_0^L \left| \frac{V(e^{-j\omega\delta T}, x)}{R(e^{-j\omega\delta T})} \right|^2 dx d\omega$ , of the primary structure under detached HVA control with respect to different locations of actuator.

Figure(s):

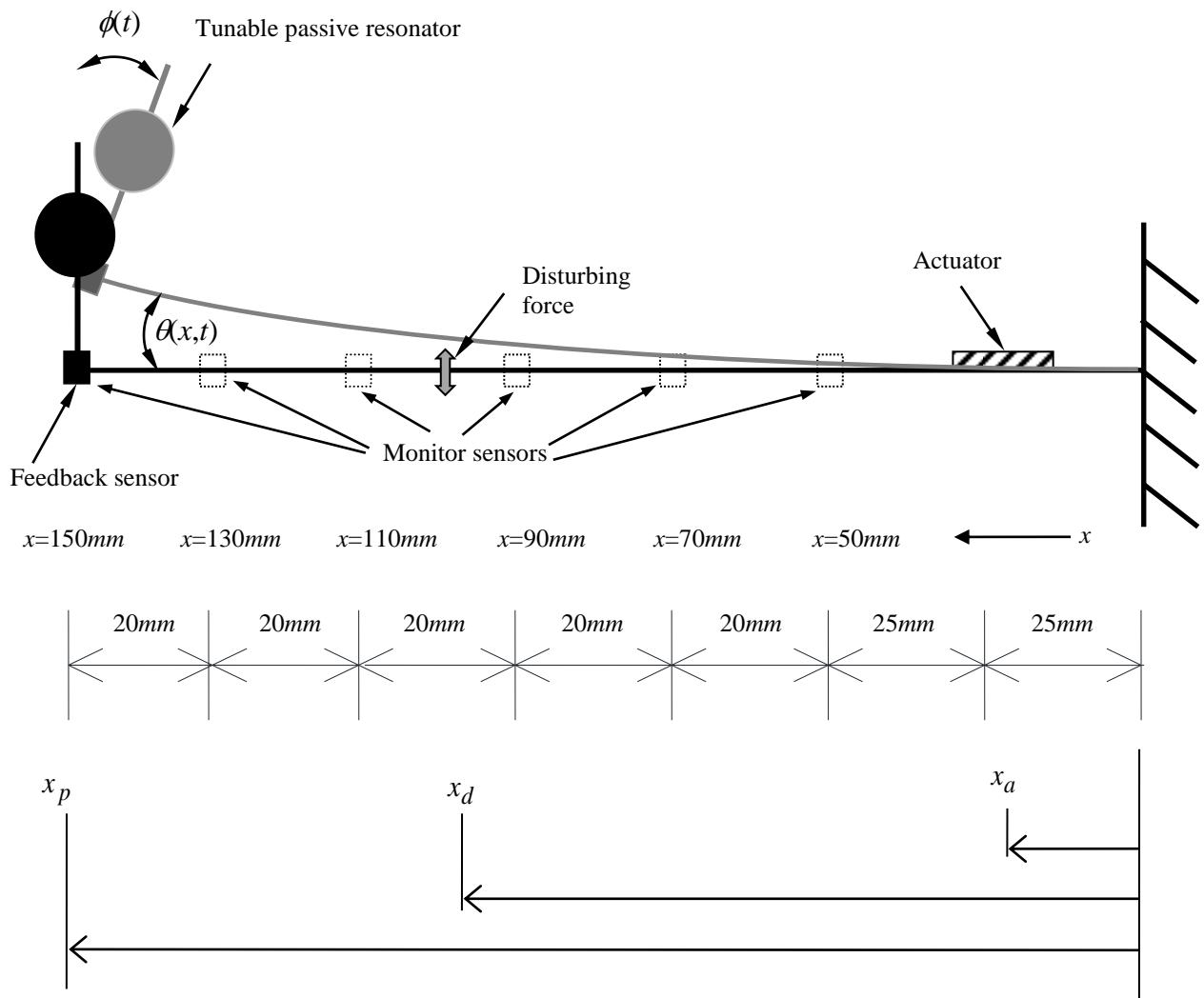


Fig. 1a Cantilever beam and detached HVA with locations of actuator ( $x = x_a$ ), resonator ( $x = x_p$ ), disturbance ( $x = x_d$ ), feedback and monitor sensors.

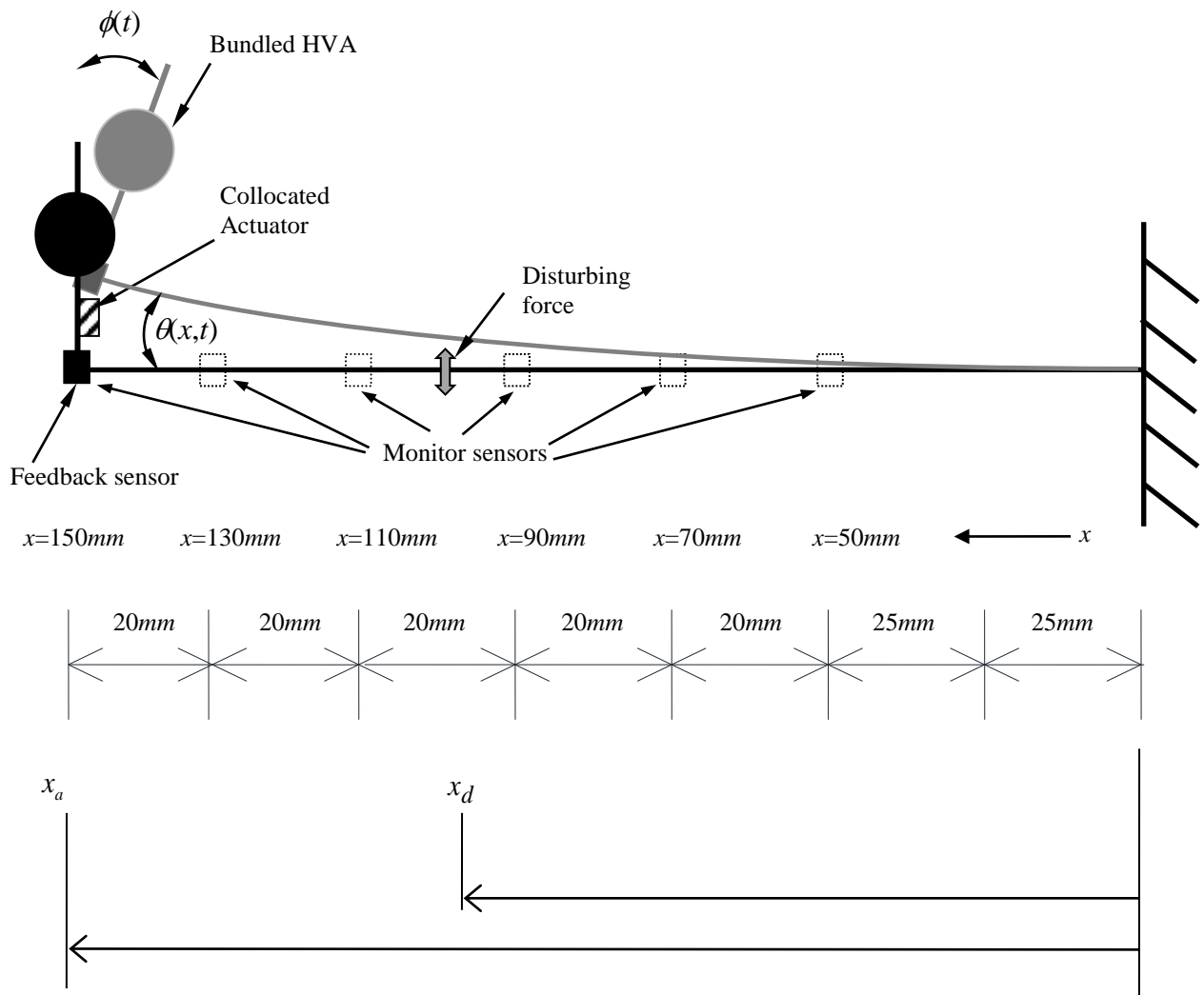


Fig. 1b Cantilever beam and bundled HVA with collocated actuator and resonator at location ( $x = x_a$ ), disturbance ( $x = x_d$ ), feedback and monitor sensors.

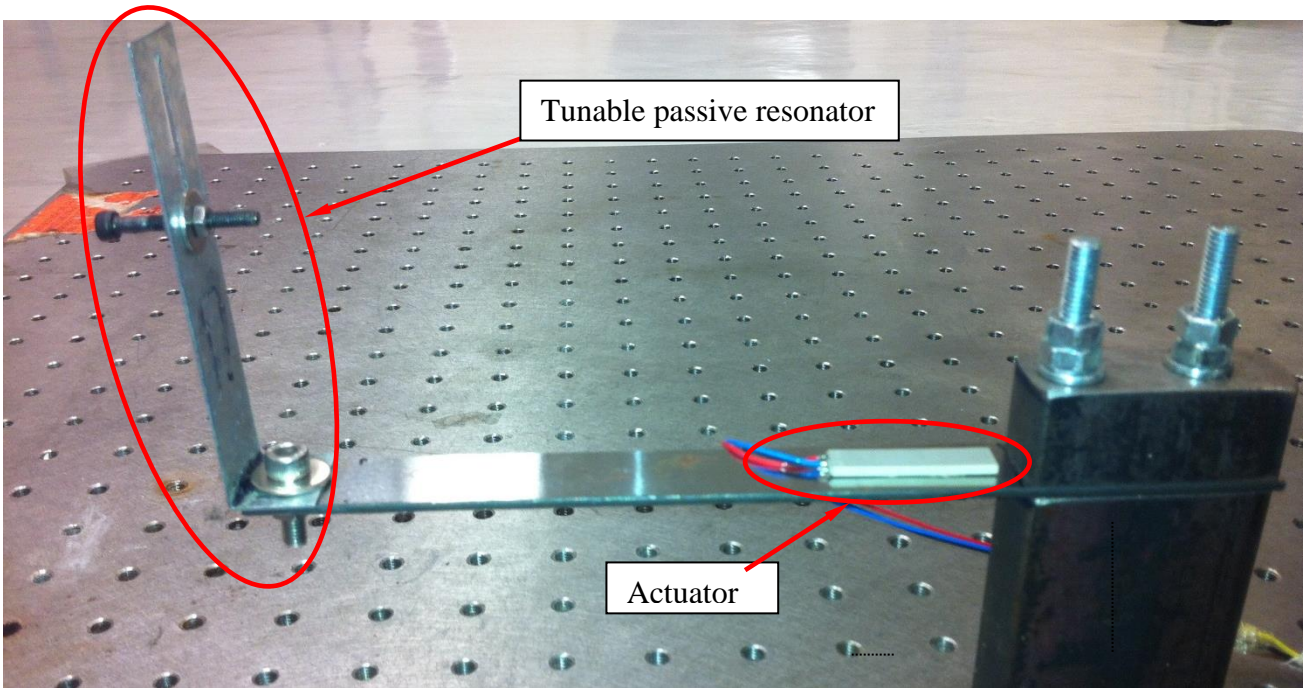


Fig. 2a Experimental rig (a cantilever beam coupled with a detached hybrid vibration absorber).

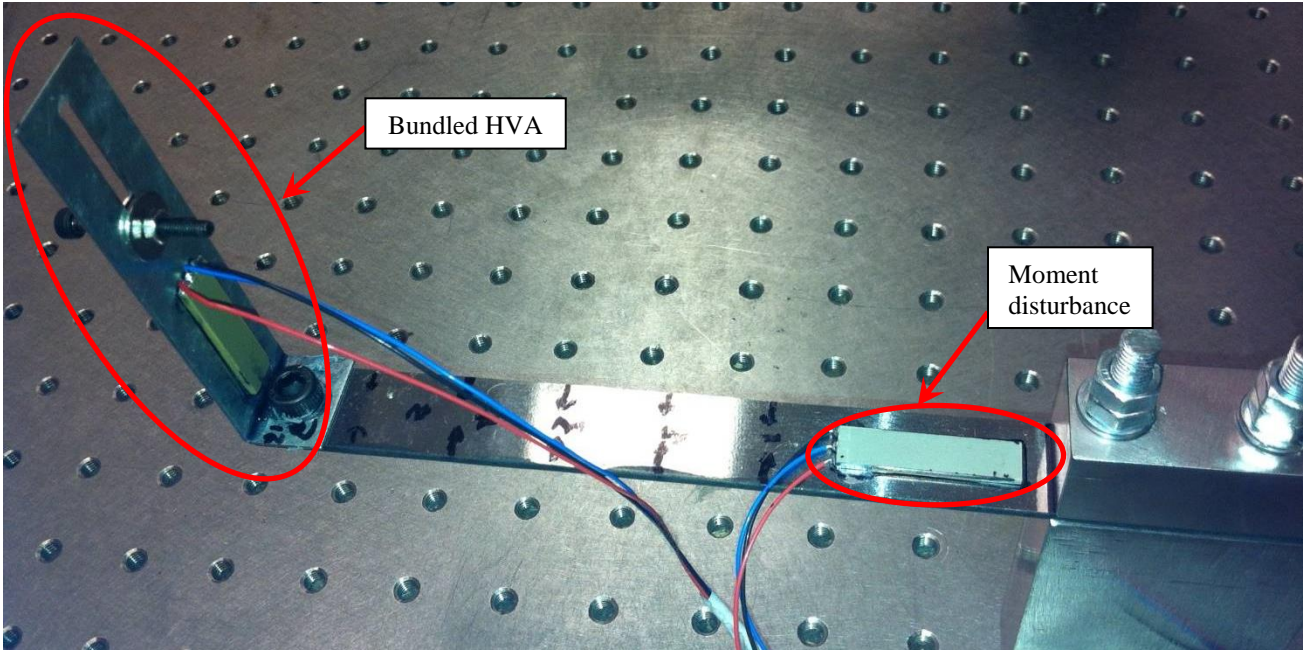


Fig. 2b Experimental rig (a cantilever beam coupled with a bundled hybrid vibration absorber).

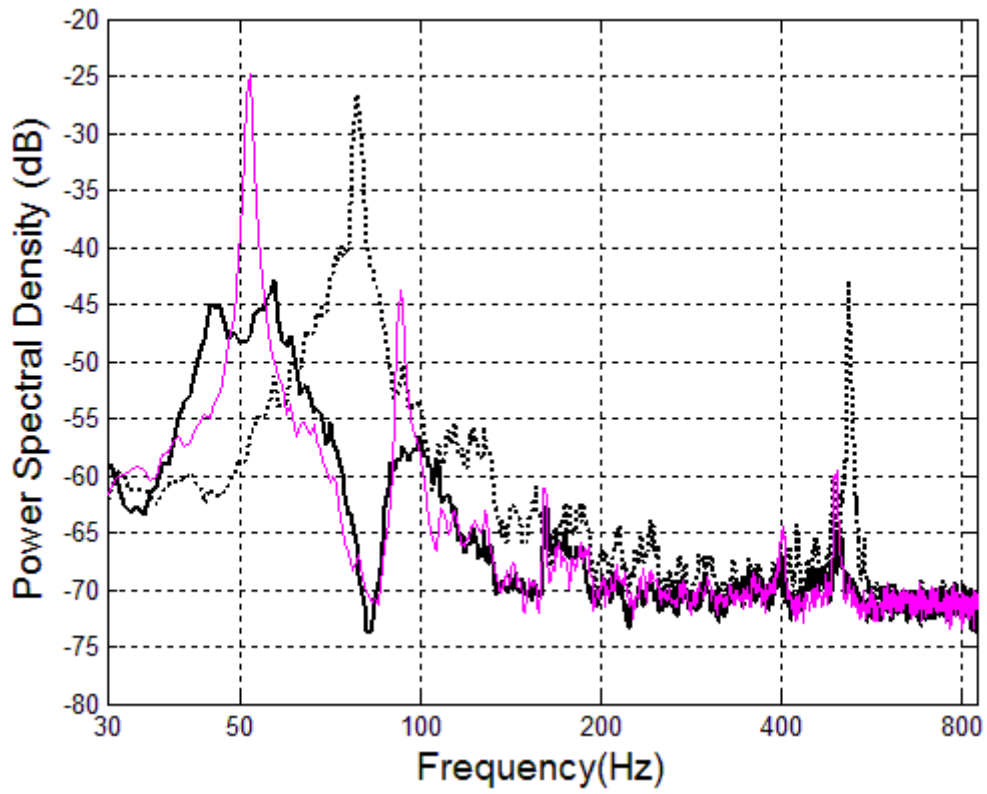


Fig. 3 Comparison of PSD,  $\left| \frac{V(e^{-j\omega\delta T}, x)}{R(e^{-j\omega\delta T})} \right|$ , measured at  $x=150mm$  of the primary structure:

..... raw beam; — with passive absorber; — with detached HVA

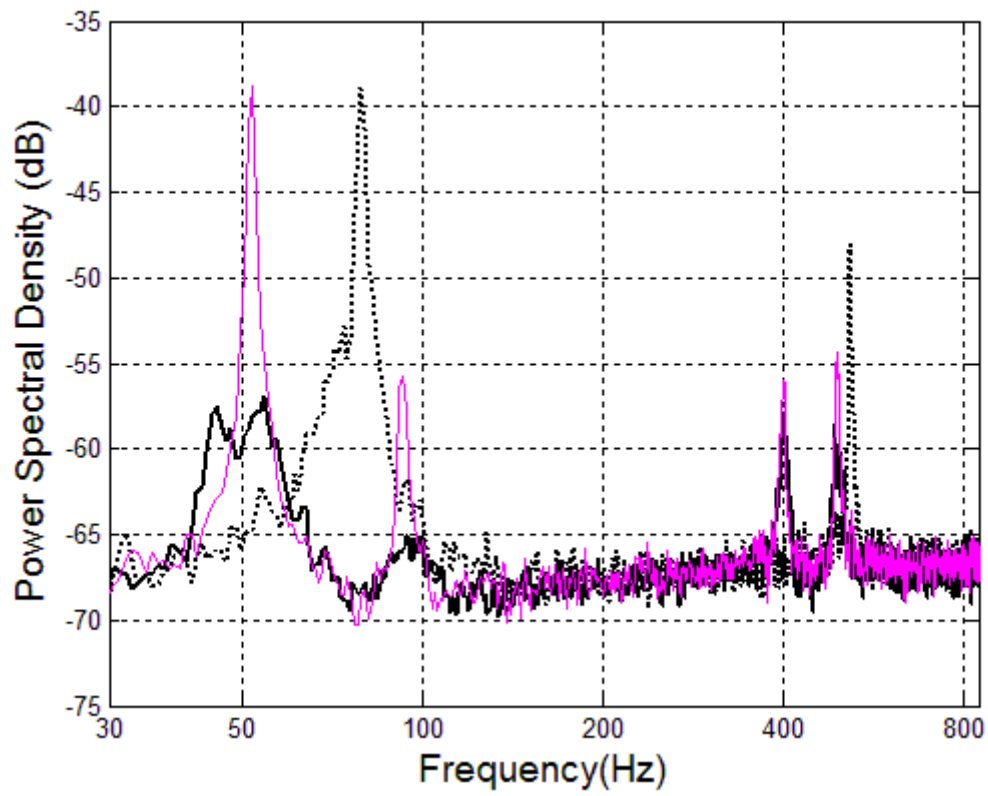


Fig. 4 Comparison of PSD,  $\left| \frac{V(e^{-j\omega\delta T}, x)}{R(e^{-j\omega\delta T})} \right|$ , measured at  $x=90mm$  of the primary structure:

..... raw beam; — with passive absorber; — with detached HVA

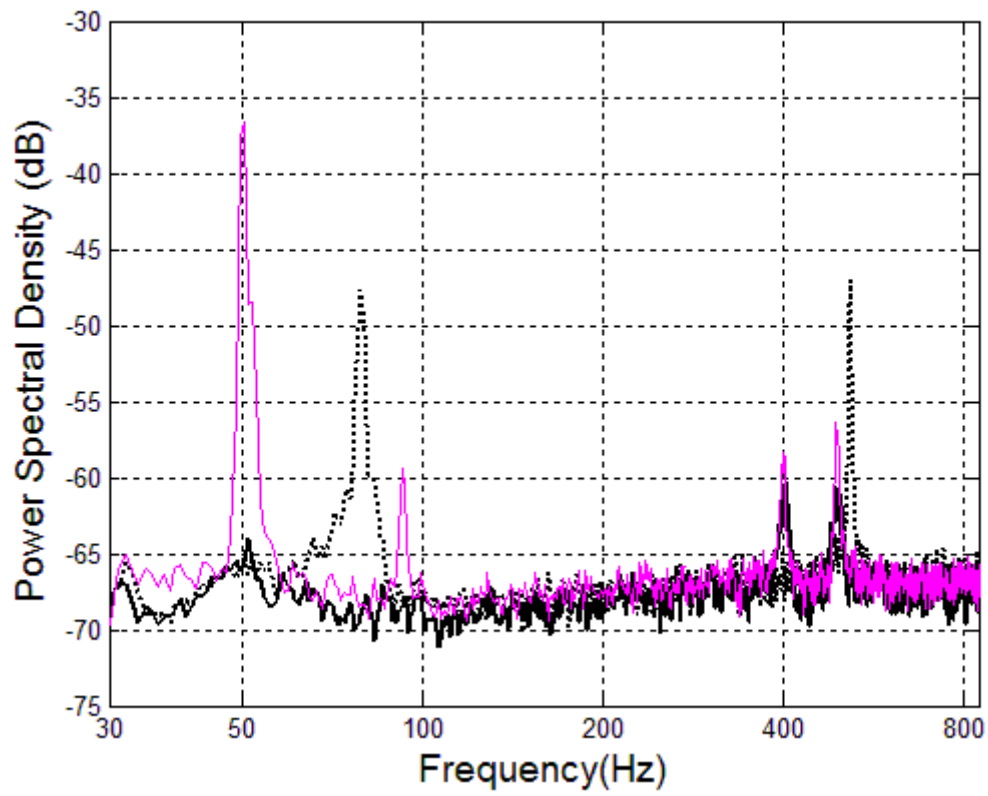


Fig. 5 Comparison of PSD,  $\left| \frac{V(e^{-j\omega\delta T}, x)}{R(e^{-j\omega\delta T})} \right|$ , measured at  $x=50mm$  of the primary structure:

..... raw beam; — with passive absorber; — with detached HVA



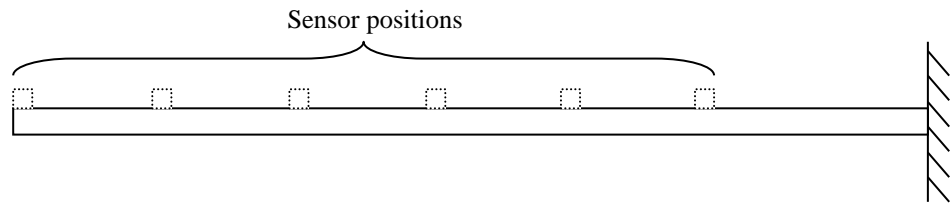
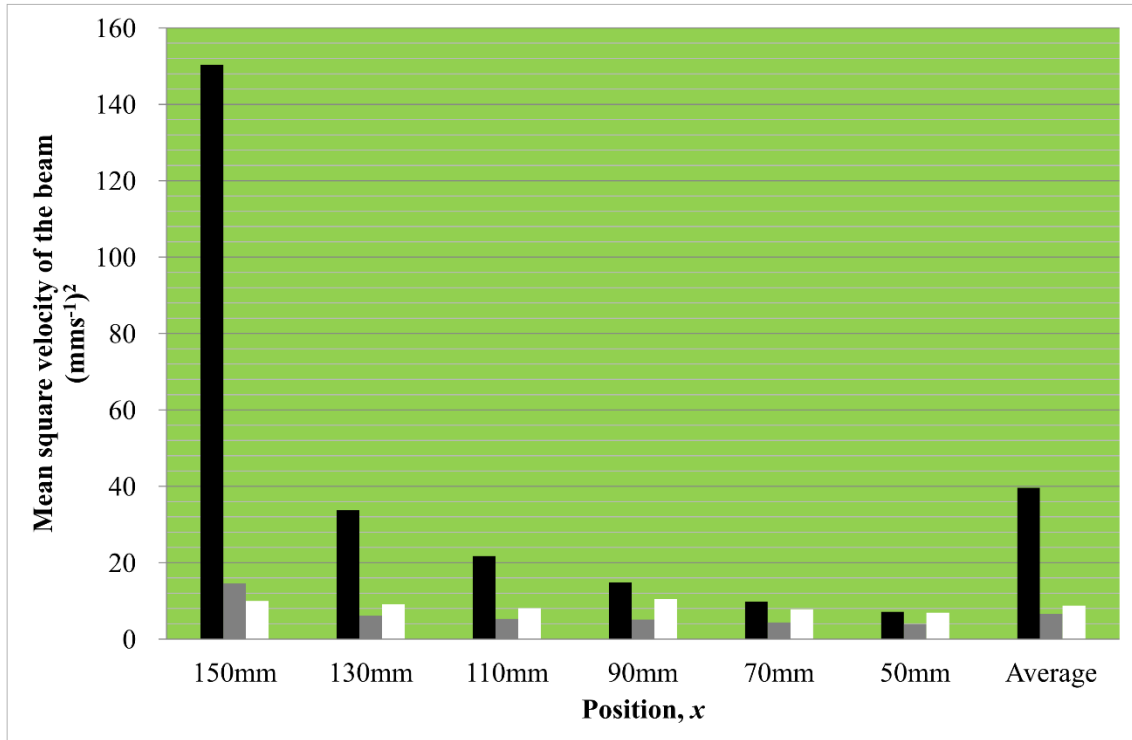


Fig. 6 Mean square velocity,  $P_x = \left(\frac{1}{N}\right) \sum_{i=1}^N v_x^2(i)$ , of the beam structure in Fig. 1a measured at  $x=150mm$ ,  $130mm$ ,  $110mm$ ,  $90mm$ ,  $70mm$ ,  $50mm$  and the spatial average value for the cases of

- (i.)  raw beam ( $P_{x\_Beam}$ ),
- (ii.)  Control with proposed “detached hybrid absorber ( $P_{x\_detached\_HVA}$ ) and
- (iii.)  Control with “bundled hybrid absorber ( $P_{x\_bundled\_HVA}$ ).

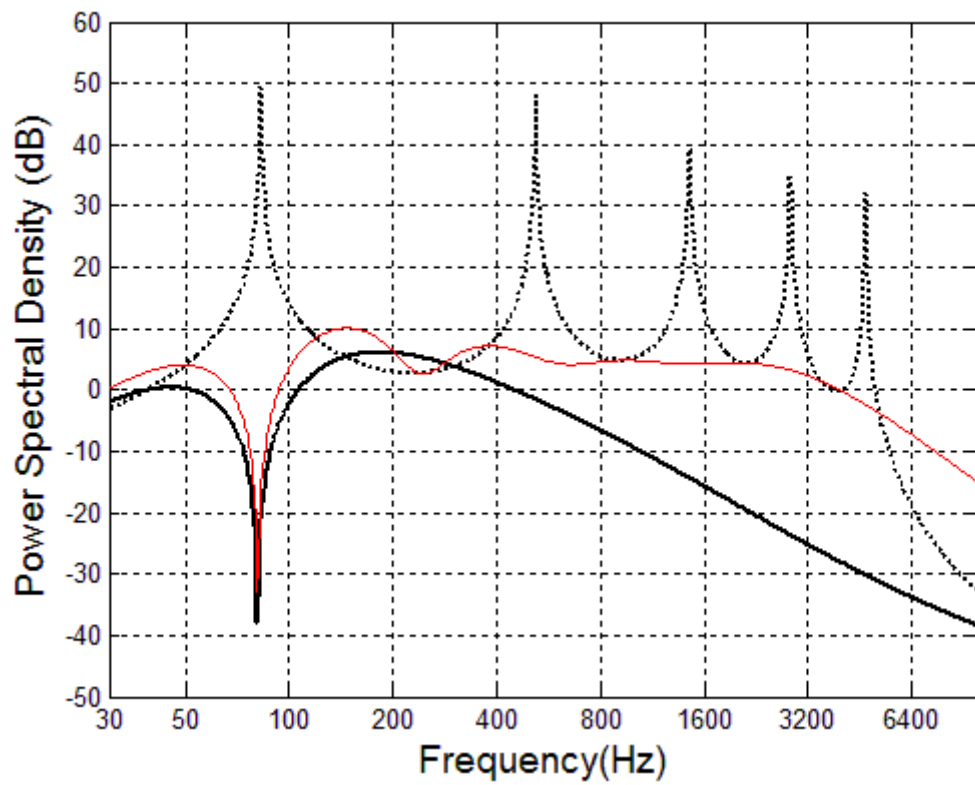


Fig. 7 Simulated vibration velocity PSD,  $\left| \frac{V(e^{-j\omega\delta T}, x)}{R(e^{-j\omega\delta T})} \right|$ , measured at  $x_m=L$  of the primary structure: - - - - raw beam; — with bundled HVA; — with detached HVA.

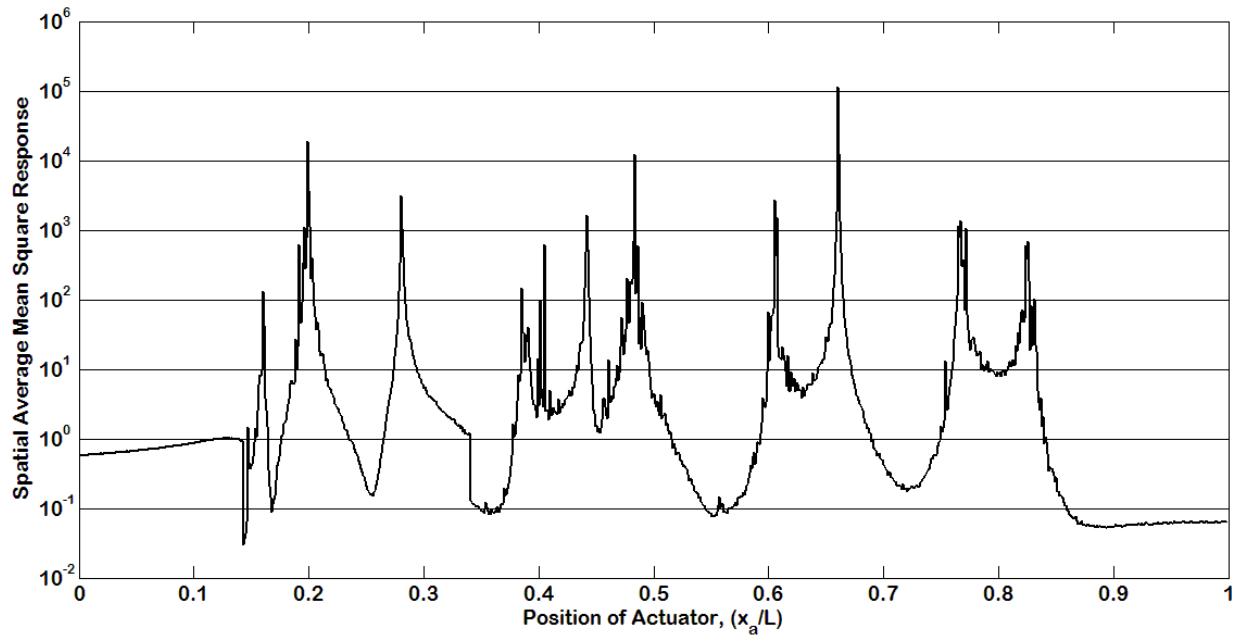


Fig. 8 Spatial average mean square response,  $\frac{1}{2\pi L} \int_{-\infty}^{+\infty} \int_0^L \left| \frac{V(e^{-j\omega\delta T}, x)}{R(e^{-j\omega\delta T})} \right|^2 dx d\omega$ , of the primary structure under detached HVA control with respect to different locations of actuator.